Research paper

EARTHQUAKE SPECTRA

Earthquake Spectra
2020, Vol. 36(2) 673–699

DOI: 10.1177/8755293019891718
journals.sagepub.com/home/eqs
SAGE

Hybrid broadband ground motion simulation validation of small magnitude earthquakes in Canterbury, New Zealand

Robin L Lee, M.EERI[1], Brendon A Bradley, M.EERI[1], Peter J Stafford, M.EERI[2], Robert W Graves, M.EERI[3] and Adrian Rodriguez-Marek, M.EERI[4]

Abstract

Ground motion simulation validation is an important and necessary task toward establishing the efficacy of physics-based ground motion simulations for seismic hazard analysis and earthquake engineering applications. This article presents a comprehensive validation of the commonly used Graves and Pitarka hybrid broadband ground motion simulation methodology with a recently developed three-dimensional (3D) Canterbury Velocity Model. This is done through simulation of 148 small magnitude earthquake events in the Canterbury, New Zealand, region in order to supplement prior validation efforts directed at several larger magnitude events. Recent empirical ground motion models are also considered to benchmark the simulation predictive capability, which is examined by partitioning the prediction residuals into the various components of ground motion variability. Biases identified in source, path, and site components suggest that improvements to the predictive capabilities of the simulation methodology can be made by using a longer high-frequency path duration model, reducing empirical V_{s30}-based low-frequency site amplification, and utilizing site-specific velocity models in the high-frequency simulations.

Keywords

Ground motion simulation, ground motion prediction, validation, new zealand, small magnitude

Date received: 21 March 2019; accepted: 8 September 2019

[1]Civil and Natural Resources Engineering, University of Canterbury, Christchurch, New Zealand
[2]Department of Civil and Environmental Engineering, Imperial College London, London, UK
[3]U.S. Geological Survey, Pasadena, CA, USA
[4]Department of Civil and Environmental Engineering, Virginia Tech, Blacksburg, VA, USA

Corresponding author:
Robin L Lee, Civil and Natural Resources Engineering, University of Canterbury, 20 Kirkwood Avenue, Christchurch 8041, New Zealand.
Email: robin.lee@canterbury.ac.nz

Introduction

Interest in using physics-based ground motion simulations for seismic hazard analysis and earthquake engineering applications has increased significantly over the past decade (Bradley et al., 2017b; Graves et al., 2011; Porter et al., 2011). The underlying physics-based nature of simulations is attractive to explicitly model salient ground motion phenomena, for example, fault rupture, wave propagation, and surficial site response. Other benefits of physics-based simulations are their ability to alleviate the paucity of large magnitude (M_w), short distance recordings by directly simulating such scenarios, and the direct provision of ground motion time series instead of intensity measures (IMs), as provided by empirical ground motion models (GMMs). However, before physics-based simulations can be widely adopted in seismic hazard analysis and earthquake engineering applications, the simulation methodologies must first be robustly validated to ensure their predictive capability approximately matches or exceeds conventional empirical GMMs.

In the past, there have been various approaches toward the validation of ground motion simulation methodologies. Validation is most commonly provided in publications alongside details of, or improvements to, their respective ground motion simulation method (e.g. Graves and Pitarka, 2010; Komatitsch et al., 2004; Mai et al., 2010; Taborda and Bielak, 2013). The above references illustrate that this type of validation is often limited to a single or few historical events. With a large focus of ground motion simulation advancements centered in Southern California, a few events are commonly considered for validation, such as the 1994 M_w 6.7 Northridge earthquake, although some other events have also taken preference in specific studies (e.g. 2008 M_w 5.4 Chino Hills earthquake (Taborda and Bielak, 2013)). The events which are usually considered are generally significant moderate-to-large magnitude events as these contribute more to hazard and have more engineering significance. However, moderate-to-large magnitude events exhibit complex phenomena, such as source rupture complexity and nonlinear site effects with larger amplitude shaking, often making it difficult to properly identify and decouple the causes of any bias. Hence the modeling of many smaller events, which do not exhibit the aforementioned complexities, can enable improved understanding of modeling for larger events under the assumption that the physical processes being represented in the simulation approach also scale appropriately to larger magnitude events. Previously, Taborda et al. (2016) simulated 30 earthquake events with $3.6 \leqslant M_w \leqslant 5.4$ in Southern California but had an emphasis on comparing the performance of various community velocity models as opposed to quantifying systematic biases and variability.

Several significant validation efforts have recently emerged in which the predictive capability of several ground motion simulation methods is tested (Dreger and Jordan, 2015; Hartzell et al., 2011; Maufroy et al., 2015). The Southern California Earthquake Center (SCEC) Broadband Platform (BBP) validation exercise rigorously evaluated four widely used simulation methods implemented on the SCEC BBP (Atkinson and Assatourians, 2015; Crempien and Archuleta, 2015; Graves and Pitarka, 2015; Olsen and Takedatsu, 2015). This exercise focused on comparing median pseudo-spectral acceleration (pSA) predictions using a one-dimensional (1D) velocity model against both recorded ground motions from historical earthquakes in different geographic regions, as well as against empirical GMMs for scenarios which are well constrained with an abundance of data (essentially testing the centering of the simulation methods) (Goulet et al., 2015). There were several exercise design decisions and imposed constraints to ensure the integrity of the validation exercise emphasizing transparency, consistency in model inputs, robustness of the validation, and more. Generally, the simulation methods performed favorably

although several shortcomings and improvements were identified (Dreger et al., 2015). The 12 events considered were all $M_w \geq 5.39$, with the exception of 1 central and eastern United States earthquake with $M_w = 4.60$.

Although the rationale for the events considered is justified and fits the purpose of the exercise, the same aforementioned limitation of omitting smaller magnitude events is present. Other limitations of this exercise include not considering non-pSA IMs, and not considering uncertainty in the prediction (also referred to as dispersion) although it is noted that these will be included in future validation exercises. Afshari and Stewart (2016b) presented a supplemental study which compared significant duration metrics from the four SCEC BBP simulation methods against the recently developed Afshari and Stewart (2016a) empirical GMM but for only five events with $M_w = 6.0 - 7.3$. The results suggested that there were shortcomings for the simulated durations.

Ground motion simulation validation efforts in New Zealand have been largely focused on the major events from the 2010–2011 Canterbury earthquake sequence, particularly the 4 September 2010 M_w 7.1 Darfield and 22 February 2011 M_w 6.2 Christchurch earthquakes (Razafindrakoto et al., 2018), and 14 November 2016 M_w 7.8 Kaikoura earthquake (Bradley et al., 2017c). However, moderate-to-large magnitude earthquakes occur relatively infrequently within a specific region. To build on previous validation efforts, small magnitude (SM) earthquakes ($3.5 \leqslant M_w \leqslant 5.0$) can be considered, and due to their frequency of occurrence, they can offer a wealth of information about systematic source, path, and site effects as a substantial number of recordings can be made at the same locations. Systematic ground motion phenomena can be examined through a non-ergodic analysis framework, where the ergodic assumption, which assumes that the variability in ground motion at a single site-source pairing is the same as the variability across the global dataset, is relaxed. While this analysis framework is most commonly utilized in empirical ground motion prediction to reduce aleatory variability (Rodriguez-Marek et al., 2011), it is also a powerful tool for evaluating the performance of any prediction method.

This article presents a comprehensive validation of the Graves and Pitarka (2010, 2015) hybrid broadband (BB) ground motion simulation methodology. This methodology is one of the simulation methods considered in the SCEC BBP validation exercise (Dreger et al., 2015; Goulet et al., 2015). Simultaneously, the Canterbury region-specific source and velocity model inputs will be validated through the ground motion simulation of SM earthquakes. The performance of selected empirical GMMs is also considered to provide a benchmark for the evaluation of the simulations. First, the earthquake sources and strong motion stations considered are presented. Next, the input models are detailed, followed by an outline of the ground motion simulation validation analysis methodology. Finally, the results of the validation are presented including an investigation of systematic source, path, and site effects.

Earthquake sources and strong motion stations considered

The Canterbury region has a wealth of ground motion data, primarily as a result of the recent 2010–2011 Canterbury earthquake sequence and the dense array of strong motion recording instrumentation. As SM earthquakes produce smaller-amplitude ground motions than large M_w earthquakes at similar distances, a rational selection process is imperative to balance quantity and quality of observational data. In this section, the selection criteria and details of the earthquake sources and strong motion stations considered

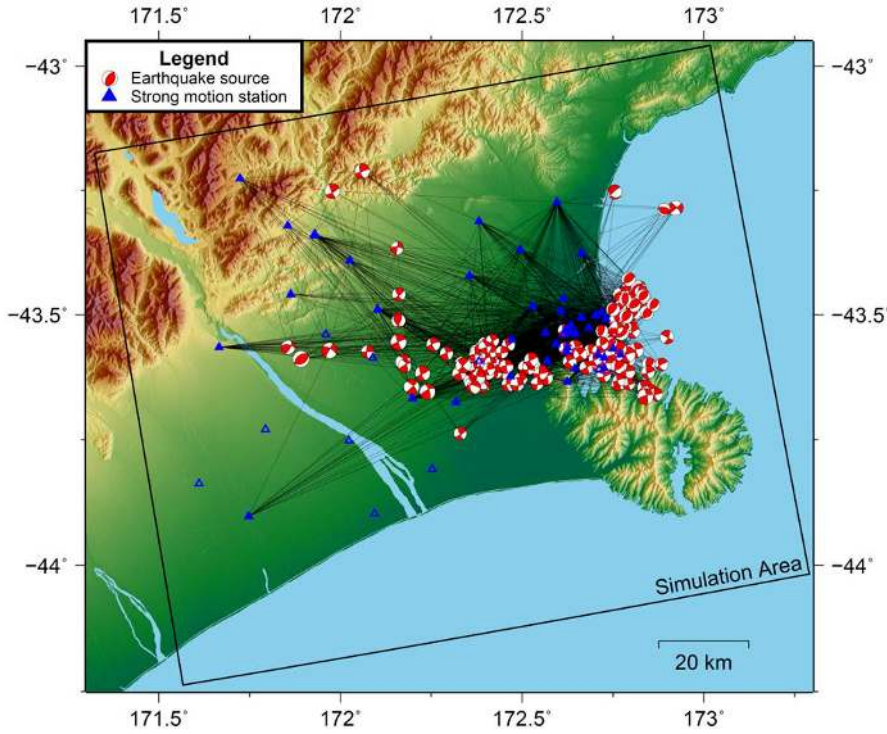

Figure 1. 148 Earthquake sources and 53 strong motion stations considered within the ground motion simulation domain. Schematic ray paths of observed ground motions are also shown as black lines. A total of 1896 ground motions satisfy the quality criteria and are used for simulation validation. Ten strong motion stations with insufficient high-quality recordings are shown as unfilled markers. Focal mechanisms are shown as lower hemisphere projections.

are presented while details of recorded ground motions and associated signal processing are presented in Electronic Supplement D.

Event and station information

Earthquake source descriptions used in this study were obtained from the GeoNet New Zealand earthquake catalogue (Ristau, 2008, see section "Data and resources"). Figure 1 presents the earthquakes considered, highlighting their spatial distribution across the region. Also shown are the location of strong motion recording stations and raypaths of ground motions considered which provides a qualitative illustration of the spatial domain being robustly assessed in the simulations. The earthquakes are densely located around the Christchurch city, Rolleston, and Darfield areas as most were aftershocks from the 4 September 2010 M_w 7.1 Darfield, and 22 February 2011 M_w 6.2, 13 June 2011 M_w 6.0, and 23 December 2011 M_w 5.9 Christchurch earthquakes (Bannister and Gledhill, 2012). Earthquakes with $M_w = 3.5 - 5.0$ were considered for this study. The minimum M_w 3.5 was chosen to ensure there is good constraint on the earthquake source parameters (specifically a centroid moment tensor solution) and adequate signal-to-noise ratio of the ground motion records. The maximum M_w 5.0 was chosen to ensure that the point source approximation is generally valid for the majority of recorded ground motions (which significantly

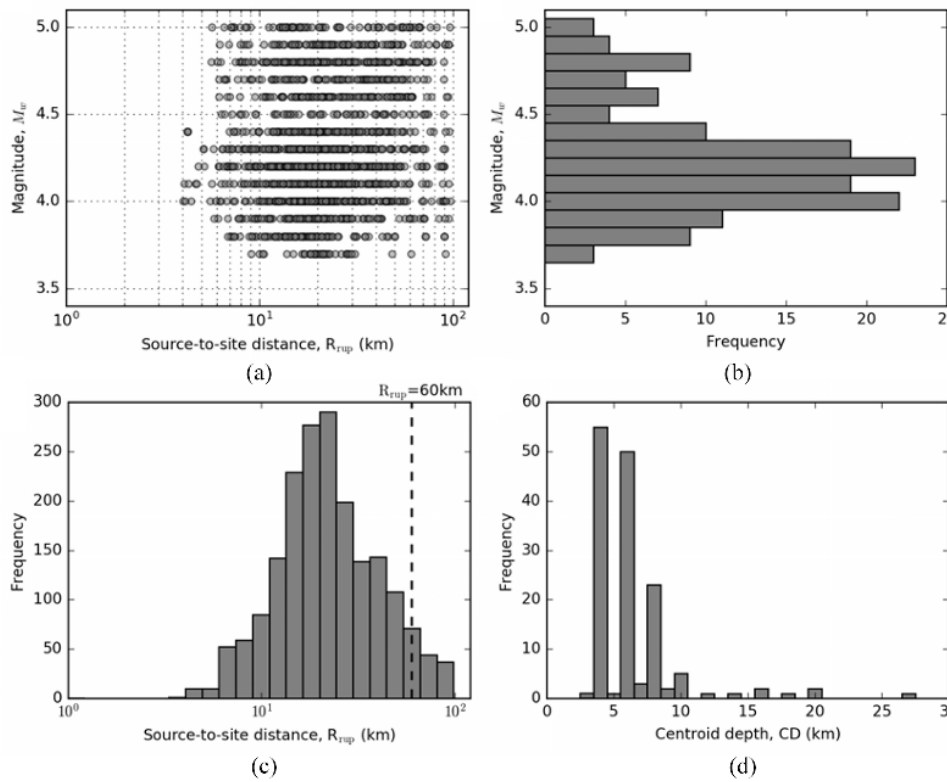

Figure 2. Earthquake source and ground motion distributions: (a) source-to-site distance versus magnitude plot, (b) magnitude distribution, (c) source-to-site distance distribution, and (d) centroid depth distribution.

simplifies the source modeling and consequent uncertainties) and that there is no appreciable off-fault nonlinear behavior in order to reduce uncertainties associated with modeling nonlinear site response. A minimum requirement of five high-quality observed ground motion records per event was also enforced (for reasons discussed subsequently) resulting in 148 earthquakes in the final dataset. Larger magnitude events generally had more high-quality ground motions. Table A.1 in Electronic Supplement A provides details of the considered events.

Figure 2 illustrates the M_w, source-to-site distance (R_{rup}), and centroid depth (CD) distributions of the considered events and recorded ground motions. Figure 2a shows the $M_w - R_{rup}$ distribution of the recordings from which it is illustrated that the database of recorded ground motions provides an approximately uniform coverage of the magnitude-distance space of interest, although the density of low magnitude, large distance records is expectedly lower. Figure 2b and d presents the distribution of M_w and CD of the 148 earthquake sources, respectively. The majority of sources are $M_w \geqslant 4.0$ and CD $\leqslant$ 10 km. The observed distribution of M_w arises as regional centroid moment tensor solutions require sufficient energy at low frequencies to invert reliable solutions. Earthquakes with $M_w \geqslant 4.0$ are routinely generated while earthquakes with $M_w < 4.0$ often do not contain sufficient low frequency energy and are therefore more selectively calculated. Of the 148 earthquakes, the rake directions indicate that the rupture mechanisms are 107 strike slip, 23 reverse, 3

normal, 12 reverse-oblique, and 3 normal-oblique. The distribution of R_{rup} for the ground motion recordings considered is shown in Figure 2c. Note that the majority of recordings have $R_{rup} \leqslant 60$ km such that small errors in the assumed anelastic attenuation are not considered significant. No maximum R_{rup} is enforced; this could lead to some bias associated with instrument triggering. However, the largest R_{rup} considered in this study are generally much smaller than those considered in other empirical GMM studies that include SM earthquakes (over 200 km, for example, Ancheta et al., 2014; Bradley, 2013; Chiou et al., 2010); thus, we do not expect that these biases would affect results. Overall, the annotated ray paths in Figure 1 provide relatively wide coverage of the Canterbury region and are significantly denser in the Christchurch city area such that some sites are better represented than others.

A total of 43 strong motion stations, whose locations are shown in Figure 1, recorded a sufficient quantity of high-quality ground motions from different events (at least five) and were considered for the purpose of examining the predictive capabilities of ground motion simulations. Table C.1 in Electronic Supplement C provides the list of stations along with their geographic coordinates, 30-m time-averaged shear wave velocity (V_{s30}), and number of earthquakes observed (NE_s). V_{s30} values are taken from Wood et al. (2011), Van Houtte et al. (2014), and Wotherspoon et al. (2014, 2015, 2016) who collectively characterized the sites through various geotechnical and geophysical techniques. The Canterbury region has a complex geology which results in the strong motion stations being located on a diverse range of site conditions, ranging from rock conditions on Banks Peninsula and the Canterbury Foothills, to gravels and marine fines in the Christchurch City and Canterbury Plains (west of Christchurch City) areas. More context on the shallow site behavior is provided with the interpretations of the analyses results. Values of V_{s30} range from 154 m/s (REHS) to 900 m/s (CRLZ), and NE_s ranges from 6 (HVSC, LPCC, and SMTC) to 136 (PPHS).

Ground motion modeling methodologies and inputs

BB ground motion simulation methodology

This study adopts the hybrid BB ground motion simulation methodology developed by Graves and Pitarka (2010, 2015, 2016) (specifically the wave propagation component of the methodology as the earthquake ruptures are modeled as point sources in this study). This method uses two different approaches for simulating the low- and high-frequency components (LF and HF, respectively) of the ground motion which are then combined in the time domain using a fourth-order Butterworth filter to produce a single BB time series. A summary of the simulation methodology pertaining to this specific study is included in Electronic Supplement E, while comprehensive details of the methodology can be found in the respective articles (e.g. Graves and Pitarka, 2010, 2015, 2016).

The ground motion simulations were performed within a computational domain of 140 km $\times$ 120 km $\times$ 46 km (whose surface projection is shown in Figure 1), with a finite difference grid spacing of 0.1 km. As the maximum resolvable frequency in the LF simulations is dependent on the grid resolution and minimum shear wave velocity, a minimum shear wave velocity of 500 m/s is enforced in the Canterbury basin to yield a maximum frequency of 1.0 Hz based on five points per wavelength for a fourth-order spatial finite difference method, which is subsequently the transition frequency where the LF and HF components are merged. This merging is performed using power spectra–based matching (as opposed to Fourier amplitude spectra–based matching, Graves and Pitarka, 2016). The simulation domain adopts the bulldozed topography approach as the Canterbury region is

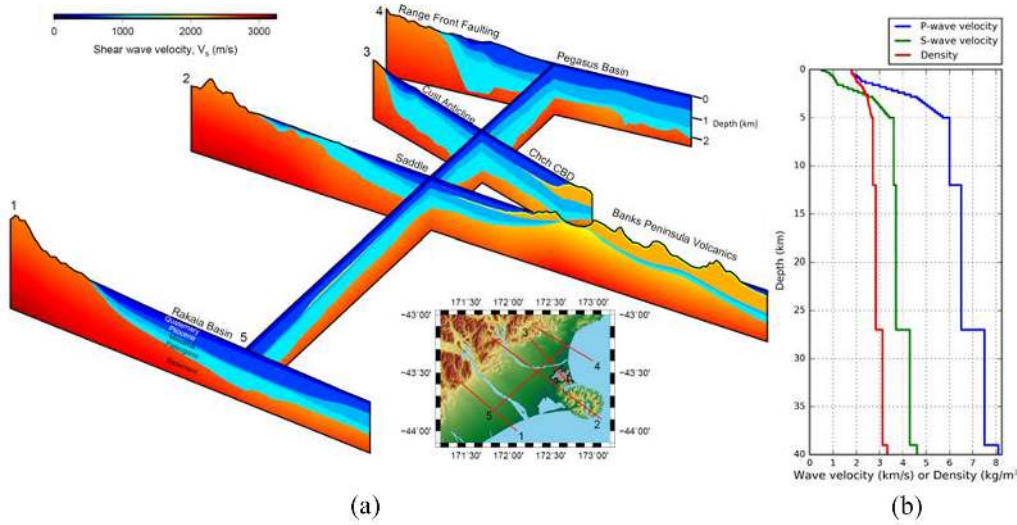

Figure 3. Crustal velocity models for ground motion simulations: (a) fence diagram of five shear wave velocity (V_s) cross sections through the 3D Canterbury Velocity Model across the Canterbury region (for LF simulations), highlighting the velocity variations and modeled geologic features; and (b) 1D velocity profiles (for HF simulations).

mostly a flat alluvial plain. A time increment of $\Delta t = 0.005$ s was utilized, matching the timestep of observed strong motion station recordings, for 20,000 time steps to produce simulated ground motions of 100-s duration for both LF and HF components.

Seismic velocity models of the region

To simulate LF ground motions, a recently developed three-dimensional (3D) Canterbury Velocity Model (CantVM; Lee et al., 2017b; Thomson et al., 2020) is used in this study to provide the P-wave and S-wave velocities, and density required (V_p, V_s, and ρ, respectively). Figure 3a presents a fence diagram of five cross sections of the CantVM through the Canterbury region which highlights the dominant regional geologic features. The CantVM explicitly models the Canterbury sedimentary basin with high spatial resolution via five distinct geologic layers. Velocities of the shallowest layer, the Quaternary unit, are prescribed from a generic regional 1D velocity model, discussed subsequently, while the other three layers are prescribed constant characteristic velocities. The depth of the sedimentary basin (i.e. depth to geologic Basement) generally ranges from around 1500–2500 m in the Canterbury Basin (Lee et al., 2017b). The Basement structure utilizes velocities from a regional-scale travel-time tomography-based seismic velocity model (Eberhart-Phillips et al., 2010) which varies smoothly with location and depth. In addition, the high-velocity Banks Peninsula volcanics, located beneath and adjacent to Christchurch city, is also explicitly modeled. The geologic features modeled have been noted in simulations of validated historical events (e.g. Bradley et al., 2017c; Razafindrakoto et al., 2018), as well as future prospective events (e.g. Bradley et al., 2017a), to strongly influence earthquake ground motions through phenomena such as basin wave-guide effects, basin-edge effects, and nonlinear soil response at frequencies of engineering interest.

For the HF component of the ground motion simulations, a regional 1D velocity model is used. Figure 3b presents the V_p, V_s, and ρ profiles which comprise the 1D velocity model.

The profiles have several low velocity and density layers in the top 3 km, and moderate velocity and density layers between 3 and 5 km, which effectively represents the sedimentary basin, while deeper layers represent geologic Basement rock. Only the top 40 km of the model are shown here as the model takes on constant values below 38 km.

Empirical ground motion IM models

In addition to the comparison between observed and simulated ground motions, the performance of selected empirical GMMs is also evaluated. The following IMs are considered: peak ground acceleration, PGA; pSA; peak ground velocity, PGV; Arias intensity, AI; and 5%–75% and 5%–95% significant durations, D_{s575} and D_{s595}, respectively. The empirical prediction models considered in this study are the Bradley (2013) New Zealand-specific GMM for PGA, pSA, and PGV; Campbell and Bozorgnia (2012) for AI; and Afshari and Stewart (2016a) for D_{s575} and D_{s595}. Justification of the choice of empirical models for the purpose of this study is presented in Electronic Supplement F.

Validation analysis methodology

Due to the large number of earthquake events considered, the analysis is primarily focused on results from considering the entire dataset of ground motions. To achieve this, the prediction residuals are partitioned into the various components of ground motion variability. A detailed comparison between observed and simulated ground motion waveforms and IMs from one event is presented in Electronic Supplement G to highlight ground motion features of the simulations.

The total prediction residual is partitioned into the various components associated with ground motion variability using a partially crossed linear mixed effects regression algorithm (Bates et al., 2015; Stafford, 2014). Following the notation of Al Atik et al. (2010), the general form of a GMM for an event, e, and station location, s, pairing can be written as:

$$\ln IM_{es} = f_{es} + \Delta \tag{1}$$

where $\ln IM_{es}$ is the natural logarithm of the observed IM; f_{es} is the median of the predicted logarithmic IM (given by either the ground motion simulation or an empirical GMM) which is a function of the earthquake rupture, e, and site location, s; and Δ is the total residual. The total residual can be further decomposed into fixed and random effects:

$$\ln IM_{es} = f_{es} + a + \delta B_e + \delta W_{es} \tag{2}$$

where a is the model bias; δB_e is the between-event residual with zero mean and variance τ^2; and δW_{es} is the within-event residual with zero mean and variance ϕ^2. Comparison of equations (1) and (2) illustrates that Δ has mean a and variance $\sigma^2 = \tau^2 + \phi^2$. δB_e represents the systematic misfit between observation and bias-corrected median prediction for a given earthquake, e. δW_{es} represents the difference between observation and the bias- and event-corrected median prediction for a ground motion record corresponding to a given earthquake, e, and site, s. Finally, δW_{es} can be further broken down into a systematic effect and a remaining residual:

$$\ln IM_{es} = f_{es} + a + \delta B_e + \delta S2S_s + \delta W_{es}^0 \tag{3}$$

where $\delta S2S_s$ is the systematic site-to-site residual, and δW_{es}^0 is the "remaining" within-event residual which represents factors which are not accounted for in the models. $\delta S2S_s$ is a zero mean random effect with variance ϕ_{S2S}^2, and δW_{es}^0 has residual variance ϕ_{ss}^2. When multiple source regions are considered, δB_e can also be decomposed into a systematic location-to-location residual and a "remaining" between-event residual. However, only one source region (Canterbury as a whole) is considered in this study; therefore, such partitioning is not undertaken and variations in δB_e are spatially continuous.

Observed systematic effects in ground motion modeling

Comparisons between observations and predictions for a single event are commonly used to provide validation and insight on a method's predictive capability. However, earthquake ground motions are known to have large variability. In order to robustly validate the systematic performance of the ground motion simulations and empirical GMMs, they are compared against observations from 148 earthquakes. In this section, the various components of ground motion variability determined using the previously presented framework (in the "Validation analysis methodology" section) are presented and discussed.

Model bias, a

Model bias is the systematic difference between observation and prediction using a specific model. In this study, this refers to either ground motion simulations or the empirical GMM for the respective IM. Figure 4 presents the model bias and total standard deviation (σ) across all events and stations considered for these prediction methods. Figure 4a illustrates that the model bias in the simulations is negative for all pSA periods indicating the simulations overpredict observed ground motions, while the Bradley (2013) empirical model also overpredicts pSA at short periods ($T = 0.01$–0.3 s), is unbiased at moderate periods ($T = 0.3$–3.0 s) and underpredicts for long periods ($T \geqslant 3.0$ s). Bradley (2015) investigated the bias of the Bradley (2013) model for large amplitude ground motions from 10 events in the 2010–2011 Canterbury earthquake sequence and found that a similar trend was evident at moderate to long periods. The simulated AI bias is relatively small while the empirical Campbell and Bozorgnia (2014) AI is severely overpredicted, with a bias value of –1.67 (although this is plotted at –1.5 for the plot to be all-inclusive) which corresponds to a factor of 5.3. This is a result of the considered earthquakes being below the model's range of magnitude applicability. Both simulated significant durations are severely underpredicted with bias values of 1.53 (corresponding to a factor of 4.6) and 1.84 (corresponding to a factor of 6.3), for D_{s575} and D_{s595}, respectively (both have been plotted at 1.5 for the plot to be all-inclusive though). The Afshari and Stewart (2016a) empirical model has effectively no bias for both D_{s575} and D_{s595}.

The simulation bias for pSA in Figure 4a has a negative dip within a localized period band, between $T = 1.0$–4.0 s, which is likely caused by the empirical V_{s30}-based site amplification for the LF ground motion (which is applied for frequencies $f = 0.2$–1.0 Hz, affecting approximately $T = 1.0$–5.0 s). The long period amplification, as recommended by Graves and Pitarka (2010), is intended to account for long period site effects when low-resolution velocity models are used that are not able to explicitly model these effects (i.e. even though the spatial discretization in the numerical simulation allows for a maximum frequency of $f_{max} = 1.0$ Hz, it is implied that the model may not adequately represent velocity variations at the corresponding spatial scales). Therefore, the appropriate level of amplification depends on the regional geology, and the resolution and quality of the

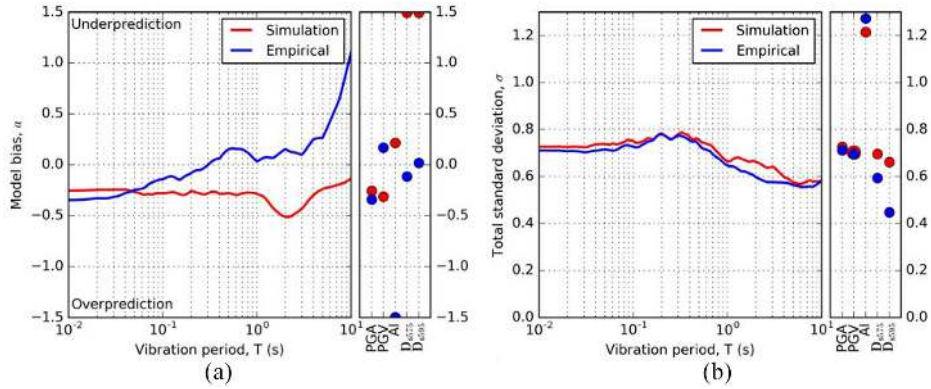

Figure 4. Simulated and empirical prediction for pSA as a function of vibration period, and five other IMs: (a) systematic model bias, a; and (b) total standard deviations, σ. Note that values which exceed the specified axis limits are plotted at the axis limits (1.5 or −1.5) for clarity and completeness, with specific values provided in the related text.

specific velocity models used. As the CantVM is used in the LF simulations, which explicitly models the Canterbury basin in high resolution, some long period site effects are explicitly modeled and therefore it is inferred that the empirical amplification is effectively "double counting" these long period site effects.

The total standard deviations, σ, of the simulation and Bradley (2013) model for pSA are similar at all vibration periods except between $T = 1.0$–4.0 s where the simulation σ is slightly larger (by roughly 7%). The σ for empirical significant durations are also lower than their simulated counterparts. The σ of all IMs, simulated and empirical, are roughly between 0.6 and 0.8 with the exception of simulated and empirical AI, which have values of 1.21 and 1.27, respectively, and empirical D_{s595}, which is the most precise IM considered. The relatively large σ for AI is consistent with previous studies (Campbell and Bozorgnia, 2012).

Between-event residual, δB_e

The between-event residuals, δB_e, are inherently associated with the location and source characteristics of each event. The present stress field of the Canterbury region typically favors inland strike-slip faulting and reverse faulting in the coastal areas (Sibson et al., 2011); hence, most sources considered in this study are strike-slip or reverse ruptures. In the ground motion simulations, the between-event variability can arise from the location of the earthquake source and kinematic source parameters which describe the fault's slip evolution. As the source models are simplified as point sources for this study, the primary factors which characterize the source model are the magnitude, location in the Earth's crust, faulting mechanism (Ristau, 2008), and HF stress parameter (Oth and Kaiser, 2014). It should be noted here that the local V_s used for calculating source slip is obtained from the 1D velocity model (and depends on the hypocentral depth) which effectively models a sedimentary basin above 5 km. The empirical GMMs considered in this study represent the source effects through magnitude scaling, depth-to-rupture measures (e.g. Z_{TOR}), and faulting mechanism modifications.

Comparison for entire dataset. Figure 5a and b presents the δB_e as a function of the considered IMs for the 148 events considered for the simulated and empirical predictions,

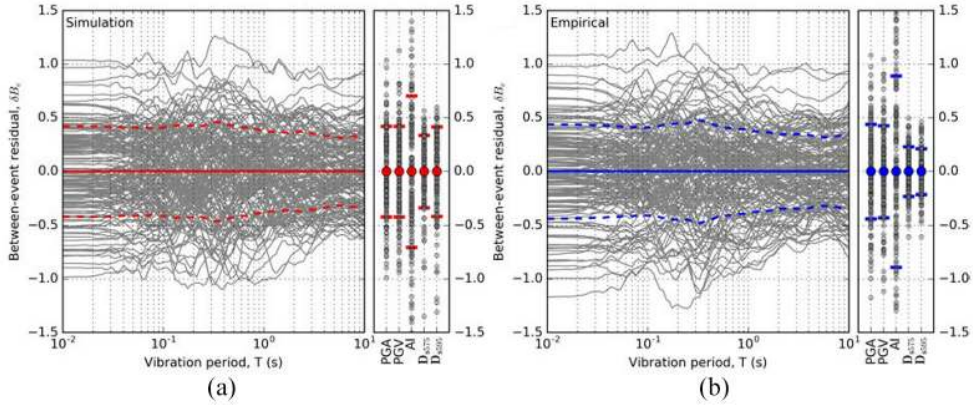

Figure 5. Computed between-event residuals for the 148 earthquakes (gray lines and points) for (a) simulated IMs and (b) empirical IMs.

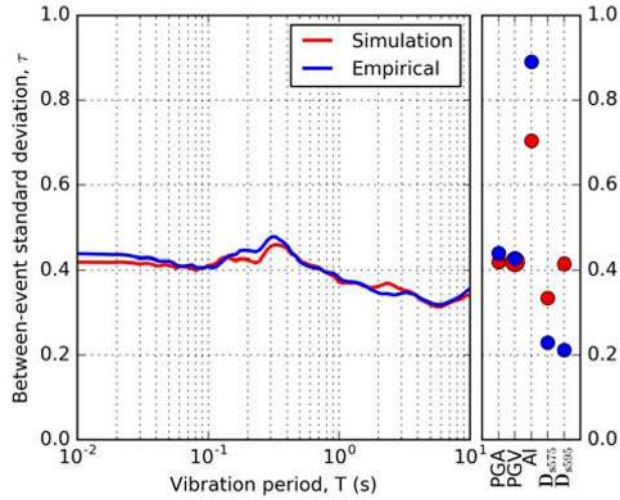

Figure 6. Between-event standard deviation, τ, for simulated and empirical predictions.

respectively. For plots of this style throughout this article, the mean and ± 1 standard deviation (τ for the between-event residuals) values are shown as the solid and dashed lines, respectively, for pSA plots and the large points and horizontal lines, respectively, for discrete IM plots. The variability and range of δB_e are similar between simulation and empirical predictions for pSA across all vibration periods considered, PGA, and PGV but different for AI, D_{s575}, and D_{s595}, each of which exhibited large model bias.

Figure 6 explicitly presents the between-event standard deviations, τ, for the simulated and empirical predictions. For pSA, PGA, and PGV, τ is practically equal between simulation and empirical prediction, with values between roughly 0.32–0.46, implying that the between-event variability is similar between the two methods. The larger values of τ occur at shorter periods while the smaller values occur at longer periods implying there is less

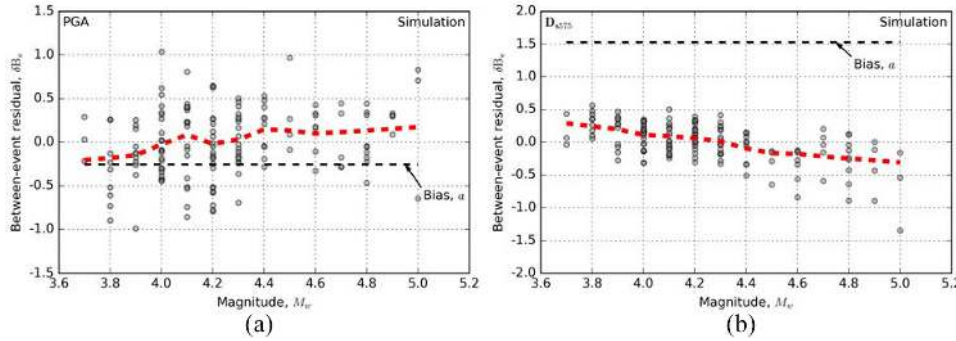

Figure 7. Comparison of simulation between-event residual against M_w for (a) PGA and (b) D_{s575}. The local linear regression trend lines are represented as the thick dashed lines, while the associated model biases, a, are represented as the thin dashed line.

variability between events at long periods. This may be a result of the spectral ordinates at the longer periods being driven by the Fourier amplitudes below the source corner frequency, so variability in factors such as stress drop is not present (although a non-trivial contributor at these periods would be the uncertainty in the focal mechanism and its mapping into the radiation pattern). The empirical predictions for significant durations have the smallest τ, at roughly 0.2 while the simulated significant durations have slightly larger τ, between 0.3 and 0.4.

Dependence on source parameters. To determine the causes of the variability and identify any bias with δB_e, the δB_e values are compared against several source parameters: M_w, CD, and focal mechanism. Here, only a subset of selected plots of simulated predictions is shown to highlight particular trends while an exhaustive set of plots is provided in Electronic Supplement I. In these plots, the average trend is also indicated qualitatively via local linear regression. Figures 7a and b provides comparisons between δB_e and M_w for PGA and D_{s575}, respectively. The comparison for PGA highlights the trend of increasing δB_e with increasing M_w. As the simulation model bias for PGA was identified as negative ($a_{PGA} = -0.25$; Figure 4), larger M_w events with positive δB_e produce more accurate predictions of PGA in an overall sense. The comparison for D_{s575} highlights the opposite trend of decreasing δB_e with increasing M_w. However, as the simulation model bias was identified as positive ($a_{D_{s575}} = 1.53$; Figure 4) for D_{s575}, larger M_w events also result in more accurate predictions of D_{s575}. While not shown here, D_{s595} also exhibits the same trend as D_{s575}. The lower bias with larger magnitude is consistent with results from validation against past large magnitude events which showed relatively small bias (Bradley et al., 2017a; Graves and Pitarka, 2010; Razafindrakoto et al., 2018).

For the simulations of SM earthquakes, the two M_w – dependent trends noted above for PGA and significant durations are inherently linked by the HF simulation duration which comprises path and source duration components. With increasing magnitude, the source duration increases such that the path duration (which remains constant for a given source-to-site distance) comprises an increasingly smaller percentage of the total duration. An increase in the total duration in this manner decreases the underprediction of significant durations, and overprediction of PGA and short period pSA. Hence, the observed biases manifest from the HF simulation path duration being too short. Consistent with

these observations, Boore and Thompson (2014, 2015) found that conventionally used path duration models used in "stochastic" simulations don't appropriately account for all factors which increase duration with distance (e.g. different arrival times for waves of varying speed, scattering, reflected, and basin waves). The significant durations of many simulated ground motions from SM earthquakes in this study are dominated by the HF acceleration amplitudes and hence demonstrate this underprediction, especially for D_{s575}. However, ground motions which have significant LF acceleration amplitudes, such as those with significant basin-induced waves, actually produce significant durations which are broadly consistent with the observations. For larger magnitude earthquakes, the biases are smaller because the HF simulation duration becomes dominated by the source corner frequency and rupture propagation over the subfaults, and the LF simulation acceleration amplitudes become significant. It should also be noted that Afshari and Stewart (2016b) found Graves and Pitarka (2010, 2015) to have distance-scaling issues, despite having relatively small bias, which may be related to the biases identified in this study. The lack of site effect consideration for duration is another source of underestimation and is elaborated upon in later sections.

Comparisons between δB_e and CD were unreliable for identifying trends as there are few earthquakes with CD below 10 km. However, it is acknowledged that the use of a constant stress parameter could cause bias with CD related to the source corner frequency and high-frequency amplitudes. For pSA(3.0 s), there appeared to be a strong tendency for 4-km deep earthquakes to be overpredicted which is inferred to be caused by lower local shear wave velocities requiring larger slip values in the source models to achieve the target moments. Shallower earthquakes also naturally have shallower incidence angles upon the Canterbury sedimentary basin boundary which can result in greater critical reflections at the basin interface. A comparison between δB_e and focal mechanism for PGA identified that reverse faulting tended to produce lower δB_e than other focal mechanisms (likely partially attributed to the use of an azimuthal-constant radiation pattern and constant stress drop). However, it should be noted that reverse faults were also mostly shallow and located in the Pegasus Bay area, and therefore this trend may be caused by bias in those factors.

Spatial dependence. Figure 8 presents a plot of the spatial variation of δB_e for simulated PGA with the observed values and a Kriged surface. Spatial plots of δB_e for other simulated IMs and the empirical predictions are included in Electronic Supplement J. The surface projections of the 4 September 2010 M_w 7.1 Darfield and 22 February 2011 M_w 6.2 Christchurch earthquake ruptures are also plotted to help infer any influence of these events on the observed $\delta \mathrm{B_e}$. The cluster of earthquakes on the easternmost segment of the Darfield earthquake rupture has primarily small or negative δB_e and is surrounded by earthquakes with positive δB_e. The offshore earthquakes to the northeast of the Christchurch earthquake with negative δB_e were aftershocks related to the 23 December 2011 M_w 5.8 and 5.9 earthquakes. It should also be noted that these offshore earthquakes were generally on shallow and reverse faults, which were previously noted to have systematically overpredicted PGA and pSA amplitudes. Again, this may be attributed to the tendency for these types of faults to have lower local V_s and stress parameters values. The results presented here are generally consistent with Trugman and Shearer (2018) who investigated 5297 earthquakes in the San Francisco Bay area between M_w = 1–4 and identified strong correlation between PGA and stress parameter values. The spatial distribution of δB_e appears to be relatively consistent between vibration periods which further indicates source properties such as the Brune stress parameter could be considered regionally variable.

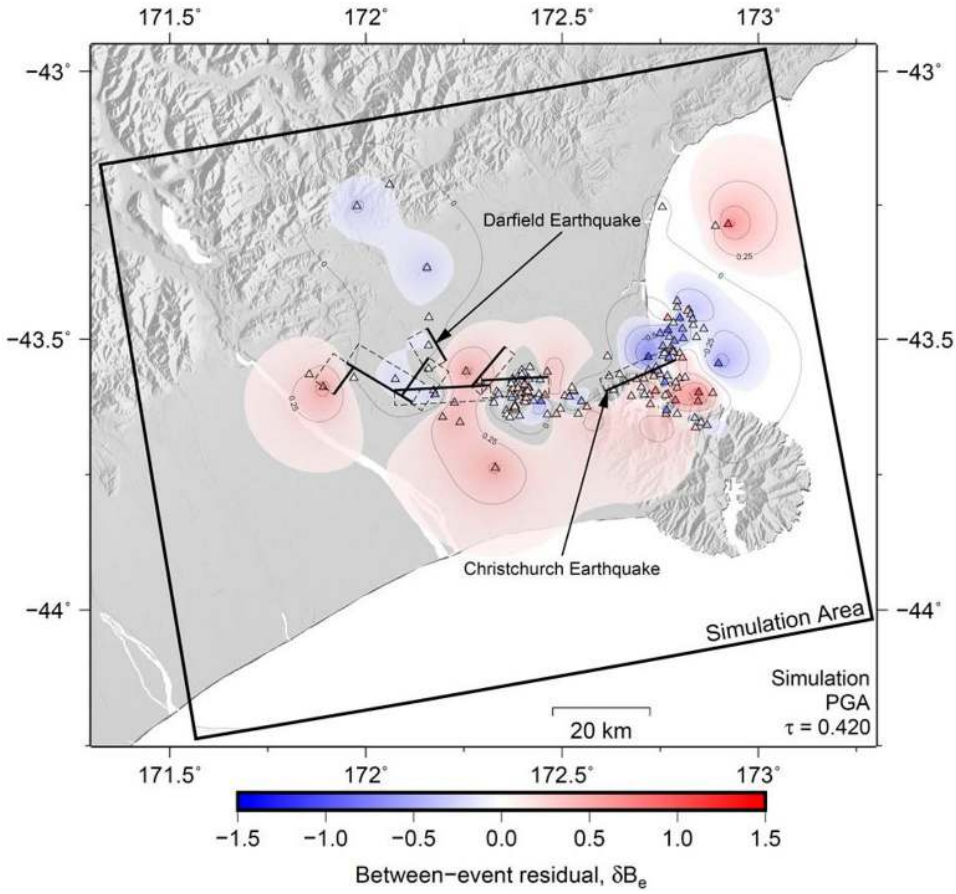

Figure 8. Spatial distribution of between-event residual, δB_e, for simulated PGA for all 148 earthquake events.

Site-to-site and within-event residuals, $\delta S2S_s$ and δW_{es}

The Canterbury region can be loosely categorized into four geographic regions with distinct geologic character: Banks Peninsula, Christchurch city, Canterbury Plains, and Canterbury Foothills. Stations located on Banks Peninsula are generally volcanic rock sites with high velocity and stiffness (Van Houtte et al., 2012). Stations located in Christchurch city are generally underlain by a sequence of interbedded marine and gravel formations, as well as the Banks Peninsula volcanics at depth, all of which can lead to complex wave propagation (Lee et al., 2017a; Wotherspoon et al., 2014, 2015). Stations located on the Canterbury Plains are mostly characterized as deep soil sites corresponding to the sedimentary deposits of the Canterbury Basin. These sites generally have gravel layers near the surface (Wotherspoon et al., 2016). Stations located in the Canterbury Foothills area are located on Basement rock or relatively thin alluvial deposits overlying Basement rock. The analyses presented here will loosely evaluate each of these categories as well as investigate specific sites where salient features are observed.

As within-event residuals are inherently associated with wave propagation path and site effects, the components of the prediction which account for these effects are the cause of

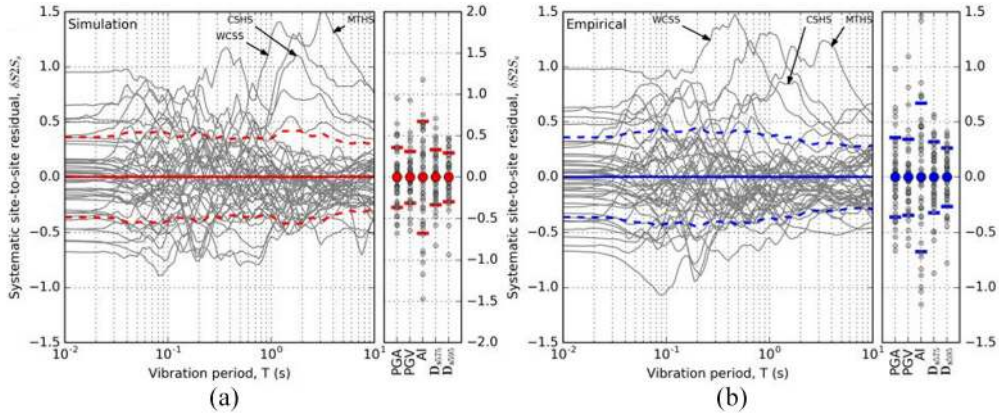

Figure 9. Computed $\delta S2S_s$ for all 43 stations considered for (a) simulated IMs and (b) empirical IMs.

any bias present in these residuals. For simulated ground motions, the path effect is dependent on the wave propagation through the specific velocity model (3D CantVM for LF and 1D velocity model for HF, as shown in Figure 3a and b, respectively). However, azimuth-specific path effects are not investigated in this study; rather, path effects are simply considered with respect to R_{rup}. Site effects are also dependent on the velocity model; however, the resolution of the velocity models used are usually unable to accurately capture the near-surface site effects. Therefore, site amplification is also applied via the V_{s30}-based shallow site response term developed by Campbell and Bozorgnia (2014). The Bradley (2013), Campbell and Bozorgnia (2012), and Afshari and Stewart (2016a) empirical GMMs all treat path effects through various source-to-site distance parameters, and site effects through V_{s30} and depth-to-rock parameters (e.g. $Z_{1.0}$ and $Z_{2.5}$, although these values have been calculated using the Abrahamson and Silva (2008) correlations with V_{s30} for this study).

Systematic site-to-site residuals for all stations. Figure 9a and b presents all $\delta S2S_s$ for the 43 strong motion stations considered for simulated and empirical predictions, respectively. The variability and range of $\delta S2S_s$ are similar between simulation and empirical predictions for pSA across all periods considered. For simulated predictions, three stations appear to have significant long period underprediction. These sites are CSHS, MTHS, and WCSS, which are all located in the Canterbury Foothill region. Although MTHS is not rock at the surface, it exhibits similar systematic site residuals to CSHS and WCSS, which are rock at the surface. There may be several factors causing this underprediction. First, the V_s of Basement rock in the CantVM, used in the LF simulations, corresponds to unweathered rock and is relatively high (e.g. $V_s = 2500$ m/s). In reality, the near-surface rock would be weathered and be lower velocity which would result in larger simulated amplitudes. Second, the three stations in question are located in the north-west of the simulation domain and only record earthquakes from a limited range of azimuths. Therefore, it is possible that systematic path effects could be included in the $\delta S2S_s$ for these sites. The corresponding empirical $\delta S2S_s$ for these three sites also exhibits large peaks but at different periods. As the features of the Canterbury Foothills sites have been discussed here, they are not included in the subsequent location-specific section.

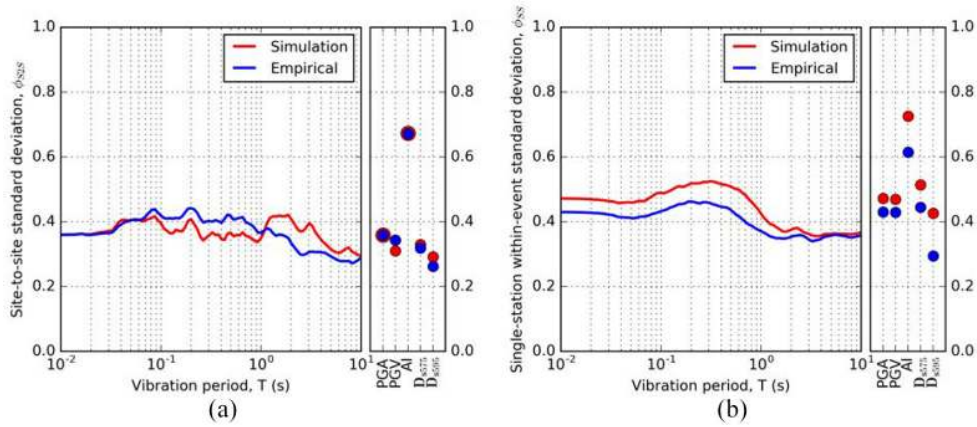

Figure 10. Within-event standard deviations: (a) systematic site-to-site uncertainty and (b) single-station within-event variability.

Figure 10a and b explicitly presents the within-event standard deviations, ϕ_{S2S} and ϕ_{ss}, respectively, for the simulated and empirical predictions which the former clearly illustrates that a significant amount of the variability between observation and prediction is the result of systematic site effects. For all IMs considered, ϕ_{S2S} are similar between simulation and empirical prediction, with values between roughly 0.30–0.45, except for pSA between $T = 1.0$–4.0 s. The larger values of ϕ_{S2S} in this range are caused by the sites at the Canterbury Foothills having significantly larger $\delta S2S_s$ than all other sites. This difference between simulated and empirical prediction ϕ_{S2S} is the primary cause of the difference in σ identified in this same period range (Figure 4). The size of ϕ_{S2S}, relative to σ, indicates that significant improvements in ground motion prediction are possible through being able to capture this systematic phenomena (Rodriguez-Marek et al., 2011). ϕ_{ss} from simulations is slightly larger than the ϕ_{ss} for empirical prediction for all IMs considered suggesting that the empirical GMMs have less unexplained variability than the ground motion simulations. It is also important to note that τ (Figure 6), ϕ_{S2S}, and ϕ_{ss} are all of similar size implying that the variability in δB_e, $\delta S2S_s$, and δW_{es}^0 are similar.

Dependence on path and site parameters. In order to evaluate the variability and biases resulting from site and path effects, the systematic site-to-site residuals, $\delta S2S_s$, are compared against V_{s30} and the "remaining" within-event residuals, δW_{es}^0, are compared against source-to-site distance, R_{rup}. As with δB_e, only a subset of comparisons for simulation residuals are presented here while an exhaustive set of plots for both simulation and empirical prediction are included in Electronic Supplement I.

Figure 11a and b presents the comparisons of $\delta S2S_s$ against V_{s30} for PGA and D_{s575}, respectively. The comparison with V_{s30} for PGA shows no significant trend while the comparison with V_{s30} for D_{s575} shows a negative trend where values are more underpredicted at low V_{s30} sites. Despite PGA and D_{s575} being strongly linked for the simulations, there is a lack of opposing trends here. This is attributed to the fact that the PGA has been modified by the period-dependent V_{s30}-based site amplification while D_{s575} has had no modification (the site effect is applied to the FAS amplitudes). Overall, the lack of site effect contributions to significant duration leads to underestimation, and is more significant for softer sites. A comparison of $\delta S2S_s$ with V_{s30} for pSA(3.0 s), not shown here, identified a positive

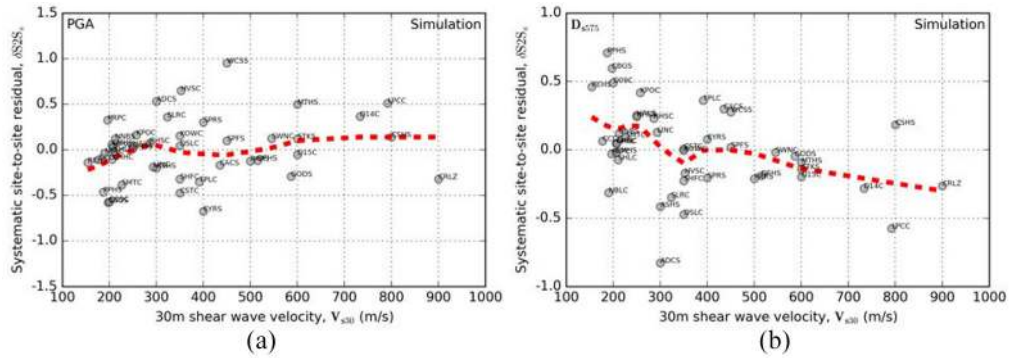

Figure 11. Comparison of simulation systematic site-to-site residual against V_{s30} for (a) PGA and (b) D_{s575}.

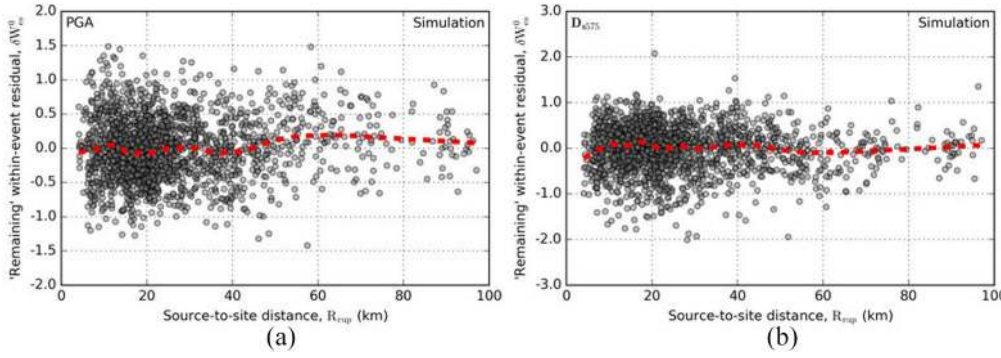

Figure 12. Comparison of simulation "remaining" within-event residual against R_{rup} for (a) PGA and (b) D_{s575}.

trend where low V_{s30} sites are more overpredicted. This is likely caused by overamplification via the period-dependent V_{s30}-based site amplification as the long period amplification is larger for softer sites.

Figure 12a and b illustrates the comparisons of δW_{es}^0 against R_{rup} for PGA and D_{s575}, respectively. For PGA, the local regression suggests that δW_{es}^0 values are slightly positive at distances beyond roughly 40 km. This feature is also apparent in pSA for all periods considered. As this bias only occurs at greater than 40 km, the most likely cause would be wave propagation effects. The comparison for D_{s575}, which is less sensitive to attenuation, shows no trend.

Spatial dependence of site-to-site and within-event residuals. Figure 13 presents a plot of the spatial variation of $\delta S2S_s$ for simulated PGA with the observed values and a Kriged surface. Spatial plots of $\delta S2S_s$ for other simulated IMs and the empirical predictions are included in Electronic Supplement J. There are many trends which are common between the PGA and pSA maps. The Canterbury Plains immediately west of Christchurch City has positive $\delta S2S_s$, while areas near or on the Canterbury Foothills, where the geologic Basement is shallow or outcrops, are negative. Negative $\delta S2S_s$ are also present for the rock sites located on Banks Peninsula or near the Banks Peninsula volcanics outcrop. In addition, at

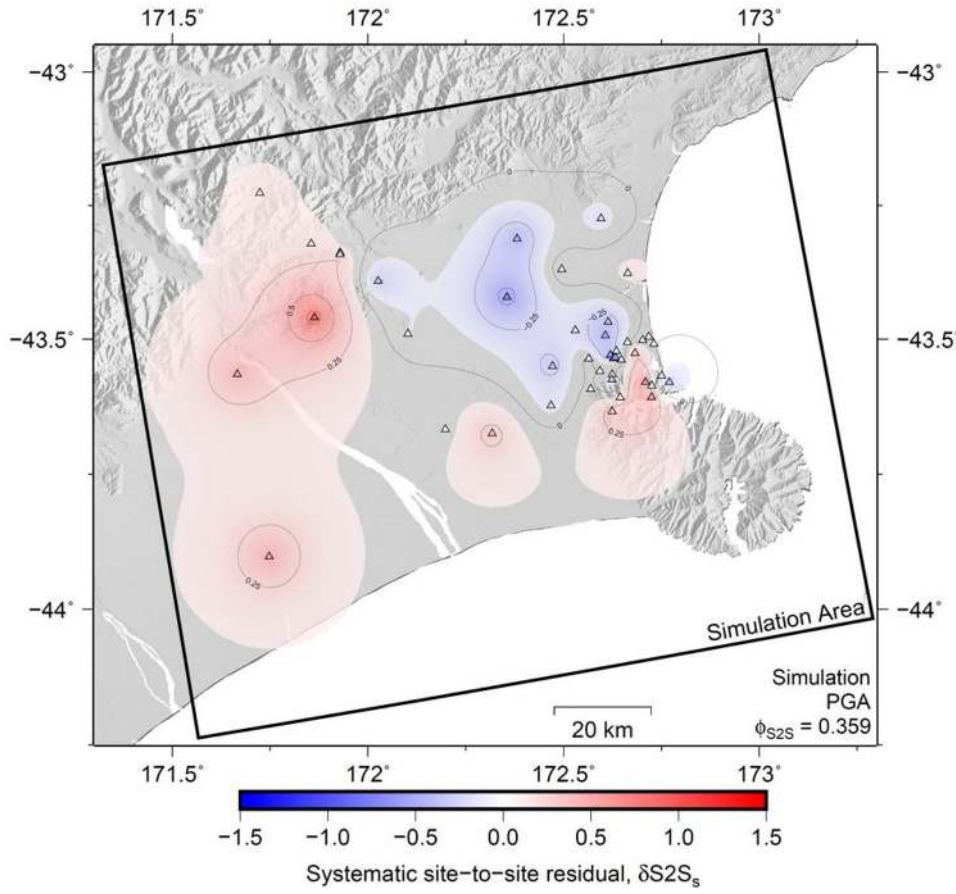

Figure 13. Spatial distribution of $\delta S2S_s$ for simulated PGA for all 43 strong motion stations.

short periods where small-scale features are significant, the Christchurch City region can be roughly separated into two areas, the western side which is overpredicted and the eastern side which is underpredicted. This segregation is mostly a result of the different surface geology where the Christchurch Formation, which mainly consists of marine sediments, is prevalent in the east and the Springston Formation, which is predominantly gravel, is prevalent in the west (Brown and Weeber, 1992). The discrepancies between velocity models and reality, particularly near-surface, suggest that explicit site response is needed although several improvements can also be made to the HF simulations to better consider site-specific characteristics (e.g. site-specific 1D velocity models and κ_0). Figure J.3b in Electronic Supplement J presents the spatial plot of $\delta S2S_s$ for pSA(3.0 s) which illustrates overprediction of long period spectral accelerations at sites located within the Canterbury Basin.

Banks Peninsula volcanic sites. Rock sites are often used as references for site response investigations as they are unlikely to be affected by nonlinear effects during large amplitude ground shaking. Figure 14a and b presents the within-event residuals (i.e. $\delta S2S_s + \delta W_{es}^0$) for the simulated predictions at the GODS and HVSC sites which have a

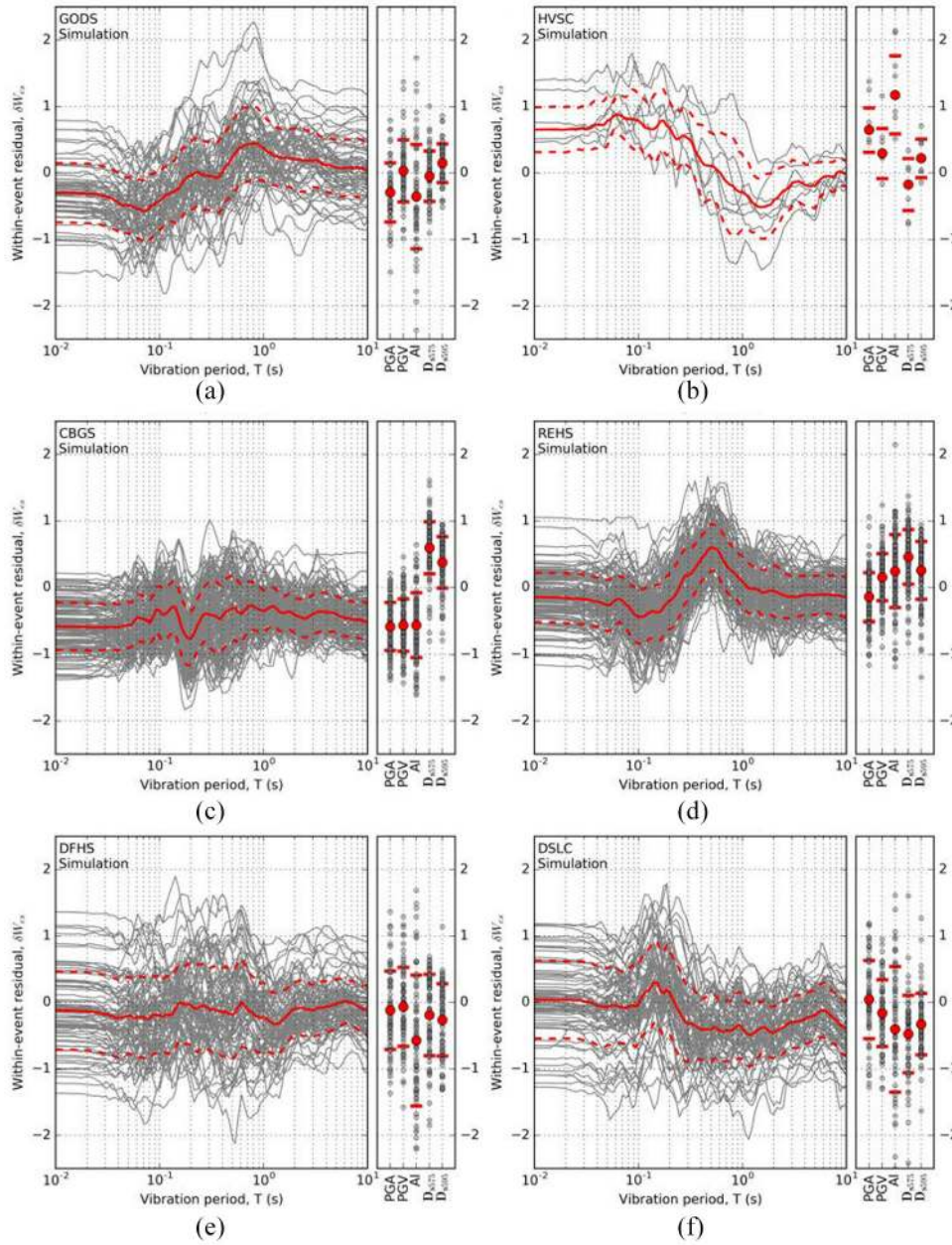

Figure 14. Computed within-event residuals, δW_{es}, for simulation prediction at sites: (a) GODS, (b) HVSC, (c) CBGS, (d) REHS, (e) DFHS, and (d) DSLC.

modeled V_{s30} of 500 and 350 m/s, respectively. In the remainder of this section, only the simulated results are discussed while the empirical results are included in Electronic Supplement K. It is noted that the empirical predictions are generally similar to the simulated results. This similarity clearly shows systematic site effects not considered via either

approach, and highlights the opportunity for improved near-surface site response modeling.

The GODS prediction exhibits a broad peak in $\delta S2S_s$ at roughly 1.0 Hz. Van Houtte et al. (2014) determined that the fundamental frequency of the GODS station was around 1 Hz through horizontal to vertical spectral ratios. Although the fundamental period is long for a rock site, Kaiser et al. (2014) investigated the site and attributed this feature to topographic effects from being located on the crest of a basaltic lava flow ridge. As the simulations and empirical models have not considered such complex topographic effects, the bias is may be attributed to this effect.

The HVSC predictions show large positive $\delta S2S_s$ at short periods ($T < 0.6$ s) and some negative values at long periods. The results found here are consistent with the findings of Razafindrakoto et al. (2016) (for simulations) and Bradley (2015) (for empirical model) in their comparisons against 10 moderate-to-large M_w events in the 2010–2011 Canterbury earthquake sequence. The observed ground motions were particularly strong at short periods due to the local geology where a thin soil layer overlying the Banks Peninsula volcanics rock results in a strong shallow impedance contrast, as well as surface waves generated at the inclined soil–rock interface (Bradley and Cubrinovski, 2011). The positive $\delta S2S_s$ at short periods manifests as neither of these features are explicitly modeled in the HF simulation or the empirical prediction. The long-period overprediction is attributed to the deamplification caused by topographic effects as investigated by Jeong and Bradley (2017).

Christchurch city sites. Figure 14c and d presents the within-event residuals for the simulated ground motion predictions at the CBGS and REHS sites which have modeled V_{s30} of 197 and 154, respectively. The two sites are located in the Christchurch Central Business District (CBD) where the surficial Christchurch Formation, consisting of marine sediments, is present resulting in low V_{s30} values. Interbedded marine and gravel formations are also expected at both sites.

At the CBGS site, many narrow-band period-dependent variations of $\delta S2S_s$ between periods of $T = 0.05$–1.0 s are present. These variations are caused by the complex observed site-specific wave propagation effects resulting from the interbedded terrestrial gravel and fine-grained marine formations, and small-scale near-surface heterogeneities, which are not modeled in the simulations or empirical model. Both also adopt a V_{s30}-based site amplification model which cannot capture these complexities and does not consider site characteristics below 30 m.

REHS has a significant positive peak at roughly $T = 0.5$–0.6 s which is consistent with the site period down to the Riccarton Gravel, located just over 20 m below the ground surface, determined from numerous studies (Wood et al., 2011; Wotherspoon et al., 2014, 2015). The underprediction manifests here as the Riccarton Gravel is not explicitly modeled in either prediction method. The amplification at this period is particularly strong as very soft surface deposits (a mix of sands, silts, clayey silts, and organic material) overlie the Riccarton Gravel at this site (Wotherspoon et al., 2014).

Canterbury Plains sites. Figure 14e and f presents the within-event residuals for the simulated ground motion predictions at the DFHS and DSLC sites located in the Canterbury Plains with modeled V_{s30} of 515 and 350 m/s, respectively. The DFHS site has small $\delta S2S_s$ for all periods considered. The degree of empirical site amplification at this site is small, so there is no significant overamplification at long periods. The DSLC site has negative $\delta S2S_s$

at long periods which is likely caused by overly strong basin waves in the simulation caused by constant velocities in the basin layers (Imperatori and Gallovič, 2017). Better characterization of velocities within the basin, such as including depth-dependence, could improve this prediction.

Discussion and conclusion

Through extensive validation using 1896 ground motions from 148 SM earthquake events recorded at 43 sites, the results from this study highlighted several limitations in the simulations – in particular (1) underprediction of significant durations, (2) overprediction of HF ground motion IMs, (3) overprediction of LF ground motion IMs, and (4) significant systematic regional variability – and suggest that some recommendations can be made to the ground motion simulation methodology utilized for the Canterbury region to improve its predictive capability, as well as other regions in general.

First, the significant durations of the simulated ground motions were severely underpredicted. The underprediction was seen to reduce with increasing magnitude, over the M_w 3.5–5.0 range considered. Such large biases in D_{s595} have not been observed in past simulations using the Graves and Pitarka (2010, 2015) method for validation over the M_w 6.0–7.5 range (Afshari and Stewart, 2016a; Razafindrakoto et al., 2018). These trends indicate that the issue lies with the path duration of the HF simulations, because for larger events the ground motion duration is dominated by the source corner frequency and rupture propagation over the subfaults. Figure 15a to c illustrates this by presenting the Husid plots of the observed and simulated CMHS 000 (north–south) ground motions from the 23 December 2011 M_w 4.9 event (examined in the illustrative example simulation in Electronic Supplement G) for LF, HF, and BB components, respectively. The simulated and observed LF ground motions have relatively similar shape resulting in similar D_{s575} and D_{s595}. Conversely, the simulated HF component has a much steeper slope than the observed HF ground motion such that the simulated D_{s575} and D_{s595} are significantly shorter than the observed. The last Husid plot illustrates that the evolution of AI in the simulated BB ground motion is dominated by the HF component, as they have similar shapes, which results in simulated D_{s575} and D_{s595} that are significantly shorter than the observed. Figure 15d presents the D_{s575} and D_{s595} bias for the BB, HF, and LF component ground motions across the entire dataset. The BB and HF values are significantly underpredicted, while the LF values are only slightly underpredicted. The slight underprediction is likely caused by the constant velocities prescribed to each sedimentary layer in the 3D CantVM, which would not adequately model the scattering of waves. Alternative formulations for the HF path duration from that in the study by Graves and Pitarka (2010, 2015) are easily usable. For example, Boore and Thompson (2014, 2015) highlighted this problem and developed a new path duration model for active crustal regions based on the NGA-West2 database which more appropriately represents factors which increase path duration with distance. Implementation of such a model would likely reduce the bias observed in significant durations. The empirical model of Afshari and Stewart (2016a) used in this article was seen to be consistent with observations, and hence the "path" component of that empirical model could also be used. In addition, the consideration of site contributions through an explicit site effect factor (such as that of Afshari and Stewart, 2016a) or a proxy such as a minimum source duration (as source durations practically saturate at the low magnitudes considered) could also reduce the underprediction. These sentiments also apply to other regions, although the extent of underprediction in significant duration may vary.

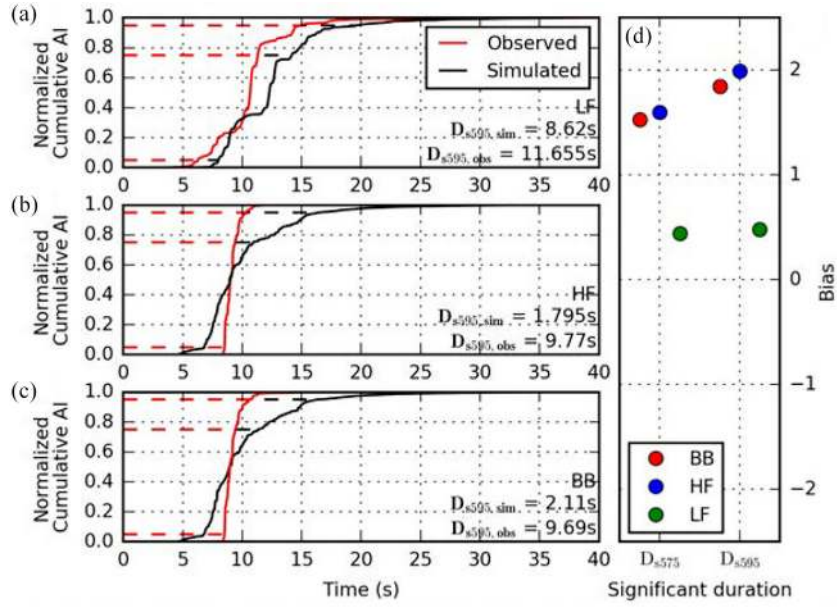

Figure 15. Husid plots for observed and simulated CMHS 000 ground motions from the 23 December M_w 4.9 event: (a) low-frequency, (b) high-frequency, (c) broadband, and (d) D_{s575} and D_{s595} model bias for each component.

The overprediction of HF amplitudes (e.g. pSA($T < 1.0$ s), Figure 4) can also be partly attributed to the HF path duration being too short because the HF simulation is based on the definition of the FAS, and it is well acknowledged that power spectral amplitudes (and consequently pseudo-spectral ordinates) will decrease as duration increases for a constant FAS (Boore, 2003). Other factors that may also affect HF simulation bias include the assumed stress parameter $\Delta\sigma$, near-surface attenuation κ_0, and anelastic attenuation.

The overprediction of LF amplitudes (e.g. pSA($T > 1.0$ s) can be partly attributed to the V_{s30}-based site amplification model applied at low frequencies. de la Torre et al. (2019) has recently shown, by comparing simulations using the same V_{s30}-based empirical site response factors or using comprehensive 1D site response wave propagation analyses, that the V_{s30}-based amplification suggested in Graves and Pitarka (2010, 2015) tends to over-amplify the long period ground motions (at least for application in the Canterbury region in conjunction with the high-resolution velocity model of Lee et al. (2017b). The overamplification demonstrated by de la Torre et al. (2019) was most significant over the T = 2.0–5.0 s range, which is also the range of largest overprediction in the simulations in this study. Reduction of the amplification at long periods, since the Canterbury Basin is explicitly modeled at relatively high resolution in the 3D CantVM, would reduce this bias. This "double counting" of site amplification is a potential problem for all regions of application and depends on how well the adopted velocity model represents the crustal structure up to the maximum resolvable frequency of the LF component. Specifically, just because the simulation is set up to achieve a certain frequency numerically doesn't mean that the velocity model is realistic to these frequencies—this is region specific, and hence underscores the importance of region-specific validation such as that performed in this study. In addition, the adopted 3D velocity model has constant velocities within discrete

sedimentary layers (Lee et al., 2017b) and, as a result, larger impedance contrasts may also contribute to overamplification. Using the V_s value from the top surface of the finite difference grid for the LF simulation reference V_{s30} in the site, amplification factor can also contribute to the overprediction as this V_s value occurs at 50-m depth (for a 100 m–spaced grid) and would be larger than a representative LF simulation V_{s30}.

The significant systematic regional variability in $\delta S2S_s$ can mostly be attributed to the assumptions and simplifications in the crustal velocity modeling. The generic 1D velocity model, anelastic attenuation, and constant κ_0 utilized in the HF simulations are all simplifications which are regionally calibrated but don't necessarily model specific sites well. The 3D velocity model used in the LF simulations, although comprehensive and high resolution, prescribes only constant velocities within most layers in the Canterbury basin. The empirical site amplification is based on V_{s30}, which itself is only a proxy parameter for site conditions. Better velocity characterization through more realistic models and more rigorous approaches should reduce this variability. The most readily implementable changes would be the use of site-specific 1D velocity profiles and κ_0 in HF simulations. The variability in $\delta S2S_s$ is expected to be similarly present in other regions, and, as examined by de la Torre et al. (2019), "geotechnical" approaches that include significantly more information on the shallow soil profile are likely necessary to significantly improve simulation prediction at HF.

The above four factors are likely to result in appreciable improvements to the simulations, all of which can be justified physically. Although the improvements were identified by investigating SM earthquakes, they will also lead to more robust predictions for large magnitude earthquakes due to the physics-based nature of the simulations. Following this, additional, less obvious, modifications may further improve the simulation predictions. With the large number of events and stations considered, the standard deviations of the components of ground motion variability were also examined to demonstrate simulation precision. The simulation and empirical prediction standard deviations were found to be similar showing that a single simulation currently gives an "average" estimate that is similar to the "average" median empirical model. This implies that the standard deviations are dominated by the underlying variability in the observations. As the improvements aim to represent the underlying physics better, they are also expected to improve simulation precision. Initial results with the modifications to the HF path duration model and reduction of long period site amplification show promise and will be more extensively detailed in future publications.

Data and resources

Earthquake source descriptions used in this study were obtained from the GeoNet New Zealand earthquake catalogue (https://github.com/GeoNet/data/tree/master/moment-tensor), recorded ground motions were obtained from the GeoNet file transfer protocol (ftp://ftp.geonet.org.nz/strong/), the 3D Canterbury Velocity Model was created using the NZVM code (https://github.com/ucgmsim/Velocity-Model), and V_{s30} values were provided by Dr Liam Wotherspoon.

The ground motion simulations were computed on New Zealand eScience Infrastructure (NeSI) high-performance computing resources using the workflow developed by the QuakeCoRE ground motion simulation team (https://github.com/ucgmsim/slurm_gm_workflow). Linear mixed effects regression was carried out using the lme4 package on RStudio. Figures were prepared using Generic Mapping Tools (http://

gmt.soest.hawaii.edu/), Python (https://www.python.org/), and Matplotlib (https://matplotlib.org/).

Acknowledgments

The authors would like to thank Hoby Razafindrakoto and Ahsan Nazer for helping with learning the ground motion simulation workflow, the QuakeCoRE Technical Platform 4 software development team, and Jeanne Hardebeck, Kyle Withers, Arthur Frankel, Morgan Moschetti, Shane Detweiler, Michael Diggles, and one anonymous reviewer for providing valuable comments on the manuscript. This is QuakeCoRE publication number 0472.

Declaration of conflicting interests

The author(s) declared no potential conflicts of interest with respect to the research, authorship, and/or publication of this article.

Funding

The author(s) disclosed receipt of the following financial support for the research, authorship, and/or publication of this article: Financial support of this research from the University of Canterbury, QuakeCoRE: The NZ Centre for Earthquake Resilience, National Hazards Research Platform (NHRP), and the Royal Society of New Zealand's (RSNZ) Marsden Fund, Rutherford Discovery Fellowship, and Rutherford Postdoctoral Fellowship are greatly appreciated. High-performance computing resources under the NeSI merit allocation are also greatly appreciated.

Supplemental material

Supplemental material for this article is available online.

References

Abrahamson N and Silva W (2008) Summary of the Abrahamson & Silva NGA ground-motion relations. *Earthquake Spectra* 24: 67–97.

Afshari K and Stewart JP (2016a) Physically parameterized prediction equations for significant duration in active crustal regions. *Earthquake Spectra* 32: 2057–2081.

Afshari K and Stewart JP (2016b) Validation of duration parameters from SCEC broadband platform simulated ground motions. *Seismological Research Letters* 87: 1355–1362.

Al Atik L, Abrahamson N, Bommer JJ, et al. (2010) The variability of ground-motion prediction models and its components. *Seismological Research Letters* 81: 794–801.

Ancheta TD, Darragh RB, Stewart JP, et al. (2014) NGA-West2 database. *Earthquake Spectra* 30: 989–1005.

Atkinson GM and Assatourians K (2015) Implementation and validation of EXSIM (a stochastic finite-fault ground-motion simulation algorithm) on the SCEC broadband platform. *Seismological Research Letters* 86: 48–60.

Bannister S and Gledhill K (2012) Evolution of the 2010–2012 Canterbury earthquake sequence. *New Zealand Journal of Geology and Geophysics* 55: 295–304.

Bates D, Mächler M, Bolker B, et al. (2015) Fitting linear mixed-effects models using lme4. *Journal of Statistical Software* 67: 1–48.

Boore DM (2003) Simulation of ground motion using the stochastic method. *Pure and Applied Geophysics* 160: 635–676.

Boore DM and Thompson EM (2014) Path durations for use in the stochastic-method simulation of ground motions. *Bulletin of the Seismological Society of America* 104: 2541–2552.

Boore DM and Thompson EM (2015) Revisions to some parameters used in stochastic-method simulations of ground motion. *Bulletin of the Seismological Society of America* 105: 1029–1041.

Bradley BA (2013) A New Zealand-specific pseudospectral acceleration ground-motion prediction equation for active shallow crustal earthquakes based on foreign models. *Bulletin of the Seismological Society of America* 103: 1801–1822.

Bradley BA (2015) Systematic ground motion observations in the Canterbury earthquakes and region-specific non-ergodic empirical ground motion modeling. *Earthquake Spectra* 31: 1735–1761.

Bradley BA and Cubrinovski M (2011) Near-source strong ground motions observed in the 22 February 2011 Christchurch earthquake. *Seismological Research Letters* 82: 853–865.

Bradley BA, Bae SE, Polak V, et al. (2017a) Ground motion simulations of great earthquakes on the Alpine Fault: Effect of hypocentre location and comparison with empirical modelling. *New Zealand Journal of Geology and Geophysics* 60: 188–198.

Bradley BA, Pettinga D, Baker JW, et al. (2017b) Guidance on the utilization of earthquake-induced ground motion simulations in engineering practice. *Earthquake Spectra* 33: 809–835.

Bradley BA, Razafindrakoto HN and Polak V (2017c) Ground-motion observations from the 14 November 2016 *Mw* 7.8 Kaikoura, New Zealand, earthquake and insights from broadband simulations. *Seismological Research Letters* 88: 740–756.

Brown LJ and Weeber JH (1992) *Geology of the Christchurch Urban Area – 1:25000* (Geological Map). Lower Hutt, New Zealand: Institute of Geological and Nuclear Sciences, p. 103.

Campbell KW and Bozorgnia Y (2012) A comparison of ground motion prediction equations for Arias intensity and cumulative absolute velocity developed using a consistent database and functional form. *Earthquake Spectra* 28: 931–941.

Campbell KW and Bozorgnia Y (2014) NGA-West2 ground motion model for the average horizontal components of PGA, PGV, and 5% damped linear acceleration response spectra. *Earthquake Spectra* 30: 1087–1115.

Chiou B, Youngs R, Abrahamson N, et al. (2010) Ground-motion attenuation model for small-to-moderate shallow crustal earthquakes in California and its implications on regionalization of ground-motion prediction models. *Earthquake Spectra* 26: 907–926.

Crempien JG and Archuleta RJ (2015) UCSB method for simulation of broadband ground motion from kinematic earthquake sources. *Seismological Research Letters* 86: 61–67.

de la Torre C, Bradley BA and Lee RL (2020) Modeling nonlinear site effects in physics-based ground motion simulations of the 2010–2011 Canterbury earthquake sequence. *Earthquake Spectra* 36(2): 856–879.

Dreger DS and Jordan TH (2015) Introduction to the focus section on validation of the SCEC broadband platform V14.3 simulation methods. *Seismological Research Letters* 86: 15–16.

Dreger DS, Beroza GC, Day SM, et al. (2015) Validation of the SCEC broadband platform V14.3 simulation methods using pseudospectral acceleration data. *Seismological Research Letters* 86: 39–47.

Eberhart-Phillips D, Reyners M, Bannister S, et al. (2010) Establishing a versatile 3-D seismic velocity model for New Zealand. *Seismological Research Letters* 81: 992–1000.

Goulet CA, Abrahamson NA, Somerville PG, et al. (2015) The SCEC broadband platform validation exercise: Methodology for code validation in the context of seismic-hazard analyses. *Seismological Research Letters* 86: 17–26.

Graves R and Pitarka A (2015) Refinements to the Graves and Pitarka (2010) broadband ground-motion simulation method. *Seismological Research Letters* 86: 75–80.

Graves R and Pitarka A (2016) Kinematic ground-motion simulations on rough faults including effects of 3D stochastic velocity perturbations. *Bulletin of the Seismological Society of America* 106: 2136–2153.

Graves R, Jordan TH, Callaghan S, et al. (2011) CyberShake: A physics-based seismic hazard model for southern California. *Pure and Applied Geophysics* 168: 367–381.

Graves RW and Pitarka A (2010) Broadband ground-motion simulation using a hybrid approach. *Bulletin of the Seismological Society of America* 100: 2095–2123.

Hartzell S, Frankel A, Liu P, et al. (2011) Model and parametric uncertainty in source-based kinematic models of earthquake ground motion. *Bulletin of the Seismological Society of America* 101: 2431–2452.

Imperatori W and Gallovič F (2017) Validation of 3D velocity models using earthquakes with shallow slip: Case study of the 2014 Mw 6.0 south Napa, California, event. *Bulletin of the Seismological Society of America* 107: 1019–1026.

Jeong S and Bradley BA (2017) Amplification of strong ground motions at Heathcote Valley during the 2010–2011 Canterbury earthquakes: The role of 2D nonlinear site response. *Bulletin of the Seismological Society of America* 107: 2117–2130Inpress.

Kaiser A, Holden C and Massey C (2014) *Site amplification, polarity and topographic effects in the Port Hills during the Canterbury earthquake sequence*. GNS Science Consultancy Report 2014/121, July. Lower Hutt, New Zealand: GNS Science.

Komatitsch D, Liu Q, Tromp J, et al. (2004) Simulations of ground motion in the Los Angeles basin based upon the spectral-element method. *Bulletin of the Seismological Society of America* 94: 187–206.

Lee RL, Bradley BA and McGann CR (2017a) 3D models of quaternary-aged sedimentary successions within the Canterbury, New Zealand region. *New Zealand Journal of Geology and Geophysics* 60: 320–340.

Lee RL, Bradley BA, Ghisetti FG, et al. (2017b) Development of a 3D velocity model of the Canterbury, New Zealand region for broadband ground motion simulations. *Bulletin of the Seismological Society of America* 107: 2131–2150.

Mai PM, Imperatori W and Olsen KB (2010) Hybrid broadband ground-motion simulations: Combining long-period deterministic synthetics with high-frequency multiple S-to-S backscattering. *Bulletin of the Seismological Society of America* 100: 2124–2142.

Maufroy E, Chaljub E, Hollender F, et al. (2015) Earthquake ground motion in the Mygdonian basin, Greece: The E2VP verification and validation of 3D numerical simulation up to 4 Hz. *Bulletin of the Seismological Society of America* 105: 1398–1418.

Olsen K and Takedatsu R (2015) The SDSU broadband ground-motion generation module BBtoolbox version 1.5. *Seismological Research Letters* 86: 81–88.

Oth A and Kaiser AE (2014) Stress release and source scaling of the 2010–2011 Canterbury, New Zealand earthquake sequence from spectral inversion of ground motion data. *Pure and Applied Geophysics* 171: 2767–2782.

Porter K, Jones L, Cox D, et al. (2011) The ShakeOut scenario: A hypothetical Mw7. 8 earthquake on the southern San Andreas fault. *Earthquake Spectra* 27: 239–261.

Razafindrakoto H, Bradley B and Graves R (2016) Broadband ground motion simulation of the 2010–2011 Canterbury earthquake sequence. In: *Proceedings of the New Zealand society for earthquake engineering conference*. Christchurch, New Zealand, 26–28 April.

Razafindrakoto HN, Bradley BA and Graves RW (2018) Broadband ground-motion simulation of the 2011 Mw 6.2 Christchurch earthquake, New Zealand. *Bulletin of the Seismological Society of America* 108: 2130–2147.

Ristau J (2008.) Implementation of routine regional moment tensor analysis in New Zealand. *Seismological Research Letters* 79: 400–415.

Rodriguez-Marek A, Montalva GA, Cotton F, et al. (2011) Analysis of single-station standard deviation using the KiK-net data. *Bulletin of the Seismological Society of America* 101: 1242–1258.

Sibson R, Ghisetti F and Ristau J (2011) Stress control of an evolving strike-slip fault system during the 2010–2011 Canterbury, New Zealand, earthquake sequence. *Seismological Research Letters* 82: 824–832.

Stafford PJ (2014) Crossed and nested mixed-effects approaches for enhanced model development and removal of the ergodic assumption in empirical ground-motion models. *Bulletin of the Seismological Society of America* 104: 702–719.

Taborda R and Bielak J (2013) Ground-motion simulation and validation of the 2008 Chino Hills, California, earthquake. *Bulletin of the Seismological Society of America* 103: 131–156.

Taborda R, Azizzadeh-Roodpish S, Khoshnevis N, et al. (2016) Evaluation of the southern California seismic velocity models through simulation of recorded events. *Geophysical Journal International* 205: 1342–1364.

Thomson EM, Bradley BA and Lee RL (2020) Methodology and computational implementation of a New Zealand velocity model (NZVM2.0) for broadband ground motion simulation. *New Zealand Journal of Geology and Geophysics* 63: 110–127.

Trugman DT and Shearer PM (2018) Strong correlation between stress drop and peak ground acceleration for recent M 1–4 Earthquakes in the San Francisco Bay Area. *Bulletin of the Seismological Society of America* 108: 929–945.

Van Houtte C, Ktenidou O-J, Larkin T, et al. (2012) Reference stations for Christchurch. *Bulletin of the New Zealand Society for Earthquake Engineering* 45: 184–195.

Van Houtte C, Ktenidou O-J, Larkin T, et al. (2014) Hard-site k0 (kappa) calculations for Christchurch, New Zealand, and comparison with local ground-motion prediction models. *Bulletin of the Seismological Society of America* 104: 1899–1913.

Wood CM, Cox BR, Wotherspoon LM, et al. (2011) Dynamic site characterization of Christchurch strong motion stations. *Bulletin of the New Zealand Society for Earthquake Engineering* 44: 195–204.

Wotherspoon L, Bradley B, Thomson E, et al. (2016) *Dynamic site characterisation of Canterbury strong motion stations using active and passive surface wave testing*. EQC Report 14/663, 30 June. Auckland, New Zealand: University of Auckland.

Wotherspoon L, Orense R, Bradley B, et al. (2014) *Geotechnical characterisation of Christchurch strong motion stations*. EQC Report 12/629, 31 October. Auckland, New Zealand: University of Auckland.

Wotherspoon L, Orense R, Bradley B, et al. (2015) Soil profile characterisation of Christchurch Central Business District strong motion stations. *Bulletin of the New Zealand Society for Earthquake Engineering* 44: 195–204.